In vivo quantitative bioluminescence tomography using heterogeneous and homogeneous mouse models

Junting Liu,[1] Yabin Wang,[2] Xiaochao Qu,[1] Xiangsi Li,[1] Xiaopeng Ma,[1] Runqiang Han,[1] Zhenhua Hu,[1] Xueli Chen,[1] Dongdong Sun,[2] Rongqing Zhang,[2] Duofang Chen,[1] Dan Chen,[1] Xiaoyuan Chen,[4] Jimin Liang,[1,*] Feng Cao,[2,*] and Jie Tian[1,3,*]

[1]Life Sciences Research Center, School of Life Sciences and Technology, Xidian University, Xi'an 710071, China
[2]Department of Cardiology, Xijing Hospital, Fourth Military Medical University, Xi'an 710032, China
[3]Institute of Automation, Chinese Academy of Sciences, Beijing 100190, China
[4]Laboratory of Molecular Imaging and Nanomedicine (LOMIN), National Institute of Biomedical Imaging and Bioengineering (NIBIB), National Institutes of Health (NIH), Bethesda 20892, Maryland, USA
**tian@ieee.org*

Abstract: Bioluminescence tomography (BLT) is a new optical molecular imaging modality, which can monitor both physiological and pathological processes by using bioluminescent light-emitting probes in small living animal. Especially, this technology possesses great potential in drug development, early detection, and therapy monitoring in preclinical settings. In the present study, we developed a dual modality BLT prototype system with Micro-computed tomography (MicroCT) registration approach, and improved the quantitative reconstruction algorithm based on adaptive *hp* finite element method (*hp*-FEM). Detailed comparisons of source reconstruction between the heterogeneous and homogeneous mouse models were performed. The models include mice with implanted luminescence source and tumor-bearing mice with firefly luciferase report gene. Our data suggest that the reconstruction based on heterogeneous mouse model is more accurate in localization and quantification than the homogeneous mouse model with appropriate optical parameters and that BLT allows super-early tumor detection *in vivo* based on tomographic reconstruction of heterogeneous mouse model signal.

OCIS codes: (170.6960) Tomography; (170.3010) Image reconstruction techniques; (170.6280) Spectroscopy, fluorescence and luminescence.

References and links

1. V. Ntziachristos, J. Ripoll, L. V. Wang, and R. Weissleder, "Looking and listening to light: the evolution of whole-body photonic imaging," Nat. Biotechnol. **23**(3), 313–320 (2005).
2. J. K. Willmann, N. van Bruggen, L. M. Dinkelborg, and S. S. Gambhir, "Molecular imaging in drug development," Nat. Rev. Drug Discov. **7**(7), 591–607 (2008).
3. F. Cao, S. Lin, X. Xie, P. Ray, M. Patel, X. Zhang, M. Drukker, S. J. Dylla, A. J. Connolly, X. Chen, I. L. Weissman, S. S. Gambhir, and J. C. Wu, "In vivo visualization of embryonic stem cell survival, proliferation, and migration after cardiac delivery," Circulation **113**(7), 1005–1014 (2006).
4. P. R. Contag, I. N. Olomu, D. K. Stevenson, and C. H. Contag, "Bioluminescent indicators in living mammals," Nat. Med. **4**(2), 245–247 (1998).
5. B. W. Rice, M. D. Cable, and M. B. Nelson, "In vivo imaging of light-emitting probes," J. Biomed. Opt. **6**(4), 432–440 (2001).
6. C. Kuo, O. Coquoz, D. Stearns, and B. Rice, "Diffuse luminescence tomography of in vivo bioluminescent markers using multi-spectral data" in *Proceeding of the 3rd International meeting of the Society* (MIT Press, 2004) p. 227.
7. J. Virostko, A. C. Powers, and E. D. Jansen, "Validation of luminescent source reconstruction using single-view spectrally resolved bioluminescence images," Appl. Opt. **46**(13), 2540–2547 (2007), http://www.opticsinfobase.org/abstract.cfm?URI=ao-46-13-2540.
8. G. Wang, E. Hoffman, G. McLennan, L. Wang, M. Suter, and J. Meinel, "Development of the first bioluminescent CT scanner," Radiology **229**, 566 (2003).

#126793 - $15.00 USD Received 9 Apr 2010; revised 16 May 2010; accepted 31 May 2010; published 3 Jun 2010

9. G. Wang, Y. Li, and M. Jiang, "Uniqueness theorems in bioluminescence tomography," Med. Phys. **31**(8), 2289–2299 (2004).
10. R. Weissleder, and M. J. Pittet, "Imaging in the era of molecular oncology," Nature **452**(7187), 580–589 (2008).
11. W. Cong, G. Wang, D. Kumar, Y. Liu, M. Jiang, L. V. Wang, E. A. Hoffman, G. McLennan, P. B. McCray, J. Zabner, and A. Cong, "Practical reconstruction method for bioluminescence tomography," Opt. Express **13**(18), 6756–6771 (2005), http://www.opticsinfobase.org/oe/abstract.cfm?URI=OPEX-13-18-6756.
12. M. Jiang, T. Zhou, J. Cheng, W. Cong, and G. Wang, "Image reconstruction for bioluminescence tomography from partial measurement," Opt. Express **15**(18), 11095–11116 (2007), http://www.opticsinfobase.org/abstract.cfm?URI=oe-15-18-11095.
13. X. Gu, Q. Zhang, L. Larcom, and H. Jiang, "Three-dimensional bioluminescence tomography with model-based reconstruction," Opt. Express **12**(17), 3996–4000 (2004), http://www.opticsinfobase.org/oe/abstract.cfm?URI=oe-12-17-3996.
14. W. Cong, H. Shen, A. X. Cong, and G. Wang, "Integral equations of the photon fluence rate and flux based on a generalized Delta-Eddington phase function," J. Biomed. Opt. **13**(2), 024016 (2008).
15. Y. Lv, J. Tian, W. Cong, G. Wang, J. Luo, W. Yang, and H. Li, "A multilevel adaptive finite element algorithm for bioluminescence tomography," Opt. Express **14**(18), 8211–8223 (2006), http://www.opticsinfobase.org/oe/abstract.cfm?URI=oe-14-18-8211.
16. R. Han, J. Liang, X. Qu, Y. Hou, N. Ren, J. Mao, and J. Tian, "A source reconstruction algorithm based on adaptive hp-FEM for bioluminescence tomography," Opt. Express **17**(17), 14481–14494 (2009), http://www.opticsinfobase.org/oe/abstract.cfm?URI=oe-17-17-14481.
17. G. Wang, X. Qian, W. Cong, H. Shen, Y. Li, W. Han, K. Durairaj, M. Jiang, T. Zhou, J. Cheng, J. Tian, Y. Lv, H. Li, and J. Luo, "Recent development in bioluminescence tomography," Current Medical Imaging Reviews **2**(4), 453–457 (2006).
18. J. Feng, K. Jia, G. Yan, S. Zhu, C. Qin, Y. Lv, and J. Tian, "An optimal permissible source region strategy for multispectral bioluminescence tomography," Opt. Express **16**(20), 15640–15654 (2008), http://www.opticsinfobase.org/oe/abstract.cfm?URI=oe-16-20-15640.
19. Y. Lu, X. Zhang, A. Douraghy, D. Stout, J. Tian, T. F. Chan, and A. F. Chatziioannou, "Source reconstruction for spectrally-resolved bioluminescence tomography with sparse a priori information," Opt. Express **17**(10), 8062–8080 (2009), http://www.opticsinfobase.org/oe/abstract.cfm?URI=oe-17-10-8062.
20. C. Qin, J. Tian, X. Yang, K. Liu, G. Yan, J. Feng, Y. Lv, and M. Xu, "Galerkin-based meshless methods for photon transport in the biological tissue," Opt. Express **16**(25), 20317–20333 (2008), http://www.opticsinfobase.org/oe/abstract.cfm?URI=oe-16-25-20317.
21. S. Ahn, A. J. Chaudhari, F. Darvas, C. A. Bouman, and R. M. Leahy, "Fast iterative image reconstruction methods for fully 3D multispectral bioluminescence tomography," Phys. Med. Biol. **53**(14), 3921–3942 (2008).
22. C. Qin, J. Tian, X. Yang, J. Feng, K. Liu, J. Liu, G. Yan, S. Zhu, and M. Xu, "Adaptive improved element free Galerkin method for quasi- or multi-spectral bioluminescence tomography," Opt. Express **17**(24), 21925–21934 (2009), http://www.opticsinfobase.org/oe/abstract.cfm?URI=oe-17-24-21925.
23. J. Feng, K. Jia, C. Qin, G. Yan, S. Zhu, X. Zhang, J. Liu, and J. Tian, "Three-dimensional bioluminescence tomography based on Bayesian approach," Opt. Express **17**(19), 16834–16848 (2009), http://www.opticsinfobase.org/oe/abstract.cfm?URI=oe-17-19-16834.
24. X. Chen, X. Gao, X. Qu, J. Liang, L. Wang, D. Yang, A. Garofalakis, J. Ripoll, and J. Tian, "A study of photon propagation in free-space based on hybrid radiosity-radiance theorem," Opt. Express **17**(18), 16266–16280 (2009), http://www.opticsinfobase.org/oe/abstract.cfm?URI=oe-17-18-16266.
25. G. Alexandrakis, F. R. Rannou, and A. F. Chatziioannou, "Tomographic bioluminescence imaging by use of a combined optical-PET (OPET) system: a computer simulation feasibility study," Phys. Med. Biol. **50**(17), 4225–4241 (2005).
26. G. Wang, W. Cong, K. Durairaj, X. Qian, H. Shen, P. Sinn, E. Hoffman, G. McLennan, and M. Henry, "In vivo mouse studies with bioluminescence tomography," Opt. Express **14**(17), 7801–7809 (2006), http://www.opticsinfobase.org/oe/abstract.cfm?URI=oe-14-17-7801.
27. M. Allard, D. Côté, L. Davidson, J. Dazai, and R. M. Henkelman, "Combined magnetic resonance and bioluminescence imaging of live mice," J. Biomed. Opt. **12**(3), 034018 (2007).
28. G. Yan, J. Tian, S. Zhu, Y. Dai, and C. Qin, "Fast cone-beam CT image reconstruction using GPU hardware," J. XRay Sci. Technol. **16**, 225–234 (2008).
29. M. Schweiger, S. R. Arridge, M. Hiraoka, and D. T. Delpy, "The finite element method for the propagation of light in scattering media: boundary and source conditions," Med. Phys. **22**(11 Pt 1), 1779–1792 (1995).
30. P. Gill, W. Murray, and M. Wright, "Practical optimization," (Academic Press, 1981).
31. H. Zhao, T. C. Doyle, O. Coquoz, F. Kalish, B. W. Rice, and C. H. Contag, "Emission spectra of bioluminescent reporters and interaction with mammalian tissue determine the sensitivity of detection in vivo," J. Biomed. Opt. **10**(4), 041210 (2005).
32. P. A. Wender, E. A. Goun, L. R. Jones, T. H. Pillow, J. B. Rothbard, R. Shinde, and C. H. Contag, "Real-time analysis of uptake and bioactivatable cleavage of luciferin-transporter conjugates in transgenic reporter mice," Proc. Natl. Acad. Sci. U.S.A. **104**(25), 10340–10345 (2007).
33. G. Wang, H. Shen, K. Durairaj, X. Qian, and W. Cong, "The first bioluminescence tomography system for simultaneous acquisition of multi-view and multi-spectral data," Int. J. Biomed. Imaging **1**, 58601 (2006).
34. D. E. Jenkins, Y. Oei, Y. S. Hornig, S. F. Yu, J. Dusich, T. Purchio, and P. R. Contag, "Bioluminescent imaging (BLI) to improve and refine traditional murine models of tumor growth and metastasis," Clin. Exp. Metastasis **20**(8), 733–744 (2003).

#126793 - $15.00 USD Received 9 Apr 2010; revised 16 May 2010; accepted 31 May 2010; published 3 Jun 2010

35. I. Kurose, S. Miura, H. Saito, S. Tada, D. Fukumura, H. Higuchi, and H. Ishii, "Rat Kupffer cell-derived nitric oxide modulates induction of lymphokine-activated killer cell," Gastroenterology **109**(6), 1958–1968 (1995).

1. Introduction

Bioluminescence imaging (BLI) has become a widely used tool for biomedical studies to enhance our understanding of diseases, to evaluate therapies, and to facilitate drug activity measurement during preclinical drug development through small animal *in vivo* imaging [1–3]. Although BLI possesses the advantages of low cost and easiness of operation [4], it does not determine depth information inside the body. It is known that light nonlinearly attenuates as a function of tumor depth and optical properties since biological tissue performs absorption and scattering characteristics [5]. In addition, planar images of weak sources near the surface may appear identical to ones produced by stronger sources deeper in the tissue [6]. BLI only indirectly reflects the activity of targeted biological object by small animal surface photon distribution [7]. Therefore, bioluminescence tomography (BLT) is required for source localization and bioluminescent source distribution inside a living small animal to produce accurate tomographic reconstructions and visualization in 3D mode [8–10].

A number of BLT algorithms have been developed in the past few years. In a simplification and approximation of radiative transfer model in biological tissue [9,11–14], several algorithms, including our improved adaptive element free Galerkin algorithm and new bayesian algorithmic framework [22,23] have been applied to allow more accurate, robust and speed reconstruction [15–21]. We also developed a photon transport model for noncontact optical imaging [24], and a new adaptive *hp* finite element method (FEM) has been used for more accurate BLT source reconstruction [16]. Despite the great progress in mathematical model and reconstruction algorithms of BLT, most of the *in vivo* studies used a homogeneous mouse model. Although some heterogeneous model studies have provided better reconstruction results based on simulations [25], such as cylindrical heterogeneous phantom [11], and real mouse model [26,27], further investigations are still needed on real heterogeneous and homogeneous mouse models for tumor-bearing. In the present paper, we compared the reconstruction results from heterogeneous and homogeneous mouse models in terms of source localization and quantification with appropriate optical parameters. Moreover, we also attempted to detect tumor at very early stage and quantify tumor cell numbers in tumor-bearing nude mouse model *in vivo*. Another important aspect of this study different from literature reports is the construction of a novel reformative dual BLT/MicroCT imaging system, facilitating easy data acquisition and co-registration.

2. Materials and methods

2.1 System design

We developed our prototype BLT/MicroCT dual modality imaging system to acquire both quantitative bioluminescence signal and high resolution anatomical readout *in vivo* in rodents. This hybrid system avoids the issue of anatomical transmogrification of co-registration between two separate BLT and MicroCT scanners. Figure 1 shows the assembly of our BLT/MicroCT hybrid system. A highly sensitive charge-coupled device (CCD) camera (Princeton Instruments PIXIS 2048B, Roper scientific, Trenton, NJ) is employed to acquire multi-view images around the mouse. A Nikon Micro-NIKKOR 55 *mm f*/2.8 manual focus lens is mounted on the CCD camera. The axial direction of the camera lens runs parallel to the precise electronic driving translation stage and vertical to the X-ray central projection direction. The MicroCT imaging is performed by employing an X-ray tube (OXFORD INSTRUMENTS series 5000 Apogee X-ray tube, X-ray technology. Inc, CA) with a focal spot size of 35 μm which is accompanied by a high-resolution flat panel X-ray detector (HAMAMATSU C7921CA-02, Hamamatsu city, Japan) incorporating a 1032 × 1012 pixel photodiode array with a 50 μm pixel pitch. It can acquire high-quality three-dimensional anatomic structure information based on Feldkamp-Davis-Kress (FDK) cone-beam reconstruction algorithm on commodity GPU using an acceleration scheme [28]. The mouse in the holder/restrainer is fixed on a computer-controlled electronic driving rotation stage. To

#126793 - $15.00 USD Received 9 Apr 2010; revised 16 May 2010; accepted 31 May 2010; published 3 Jun 2010

perform the BLT experiment in a totally dark environment, the complete prototype BLT system is covered upside down with an extremely light tight chamber. A Matrx VIP 3000 anesthesia machine (Matrix Medical Inc, MN) is employed to keep mouse sedated during the experiment to provide rapid control of anesthetic depth and little resistance to respiration.

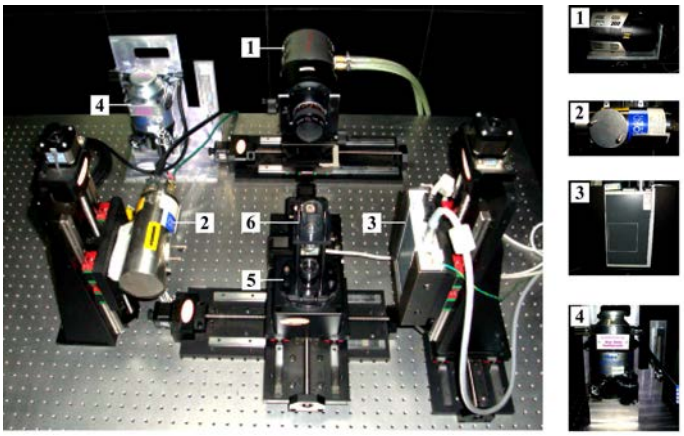

Fig. 1. Our prototype BLT/MicroCT dual modality imaging system. (1) CCD camera. (2) X-ray tube. (3) X-ray detector. (4) Anesthesia machine. (5) Rotation stage. (6) Mouse holder.

2.2 Quantitative reconstruction algorithm based on hp-FEM

Our prototype BLT system works in continuous wave (CW) mode, photons propagation in the diffusion media can be well described by the steady-state diffusion equation [29],

$$-\nabla\cdot\left(D(\mathrm{x})\nabla\Phi(\mathrm{x})\right)+\mu_a(\mathrm{x})\Phi(\mathrm{x})=S(\mathrm{x})\quad(\mathrm{x}\in\Omega),\tag{1}$$

where Ω is the region of interest, $\Phi(\mathrm{x})$ represents the photon flux density at location x $[Watts/mm^2]$, $S(\mathrm{x})$ denotes the internal source density $[Watts/mm^3]$, $\mu_a(\mathrm{x})$ is the absorption coefficient $[mm^{-1}]$, $D(x)=\left(3\left(\mu_a(\mathrm{x})+\left(1-g\right)\mu_s(\mathrm{x})\right)\right)^{-1}$ is the optical diffusion coefficient $[mm]$, $\mu_s(\mathrm{x})$ is the scattering coefficient $[mm^{-1}]$, and g is the anisotropy parameter.

In our experimental luminescence data acquisition, the light tight chamber can ensure an ideal dark environment, so Robin boundary condition can be performed [29].

$$\Phi(\mathrm{x})+\frac{2(1+R(\mathrm{x}))}{1-R(\mathrm{x})}D(\mathrm{x})(\upsilon(\mathrm{x})\cdot\nabla\Phi(\mathrm{x}))=0\quad(\mathrm{x}\in\partial\Omega),\tag{2}$$

where $R(x)$ can be approximated with $R\approx-1.4399n^{-2}+0.7099n^{-1}+0.6681+0.0636n$ [29], n is the refractive indices. In the past several years, conventional FEM has been extensively applied in BLT reconstruction [11,15,16,21,26]. Recently we recognized the advantages of *hp*-FEM approach in localization and quantification for adaptive mesh refining [16]. At the same time, *hp*-FEM strategy can improve the reconstructed robustness and reduce the ill-posedness in BLT reconstruction.

In this adaptive *hp*-FEM framework, the continuous field $\Phi(x)$ can be discretized with its values at a finite number of points in Ω as follows:

$$\Phi(x)\approx\Phi^k(x)=\sum_{i=1}^{N}\phi_i^k(x)\Psi_i^p(x),\tag{3}$$

#126793 - $15.00 USD Received 9 Apr 2010; revised 16 May 2010; accepted 31 May 2010; published 3 Jun 2010

where N is the number of interpolation basis functions, ϕ_i^k is the ith nodal value on the kth level, $\{\Psi^1(x), \Psi^2(x), \cdots, \Psi^p(x), \cdots\}$ were considered as the basis functions with different orders at different mesh levels.

Similarly, the source $S(x)$ is discretized on the same finite element mesh as [16]:

$$S(x) \approx S^k(x) = \sum_{i=1}^{N} s_i^k(x)\gamma_i^p(x), \tag{4}$$

where s_i^k and $\gamma_i^p(x)$ are the nodal values and interpolation basis functions on the kth level, respectively. The selection of interpolation basis functions $\gamma^p(x)$ may be the same with that of nodal basis functions $\Psi^p(x)$.

Equation (1) and Eq. (2) can be reduced to the following matrix form as [16]:

$$A_k S_k^{Per} = \Phi_k^B, \tag{5}$$

where S_k^{Per} are the source values of the permissible source region, which is marked according to a *priori* knowledge, Φ_k^B represents the nodal flux density on the boundary which can be measured $\partial\Omega$, $A_k = \left(M_k^{11} - M_k^{12}\left(M_k^{22}\right)^{-1}\left(M_k^{12}\right)^T\right)^{-1}(F_k^{11} - M_k^{12}\left(M_k^{22}\right)^{-1}F_k^{21})$.

Because Eq. (5) is difficult to solve since the ill-posed nature of BLT, so we adopted the classical Tikhonov regularization method to handle it and the following equation determines reconstructed source distribution [16].

$$\min_{S_{\inf} \le S_k^{per} \le S_{\sup}} \Theta(S_k^{per}) = \left\{\left\|A_k S_k^{per} - \Phi_k^B\right\|_\Lambda + \lambda_k \eta(S_k^{Per})\right\}, \tag{6}$$

where $S_{\inf}$ and $S_{\sup}$ are the lower and upper bounds of the source density, Λ is the weight matrix, and $\|V\|_\Lambda = V^T \Lambda V$, λ represents the regularization parameter, $\eta(\cdot)$ is the penalty function.

In the computation of our mouse models, a modified Newton method and active set strategy were adopted to solve the minimization problem [9,30].

Furthermore, in order to obtain the quantitative reconstruction result we also calibrated our CCD camera by an integrating sphere of 12 inches in diameter (USS-1200V-LL Low-Light Uniform Source, Labsphere, North Sutton, NH). Our calibrated camera is used for data acquisition of luminescent images on mouse surface, the image pixel gray level can reveal the mouse surface power or photon flux information. At the same time, we consider the field of view and the distance from detector plane of the CCD camera to the mouse surface in our calibration work. The relationship involves the image pixel gray value, the exposure time and the position parameters, etc., and the final calibration formula for the CCD camera is given by

$$E = [\frac{0.0001(v+20)}{t_e} + 0.0009] \times \frac{(R-d)\times 59.72}{5.7R}, \tag{7}$$

where E (nW/mm^2) is the irradiance intensity on the mouse surface, v is the pixel gray value of the luminescent image from CCD camera, t_e (Sec) is the exposure time for the luminescent images acquisition. R (mm) is the distance from the mouse surface to the edge of cylindrical lens, and d (mm) is the distance from the mouse surface to the center of lens front face.

In addition, several nude mouse models with different tumor cell numbers were reconstructed to correlate the cell number with total power. Total power was defined as integration of the reconstructed flux intensity over all elements in the permissible source region.

#126793 - $15.00 USD Received 9 Apr 2010; revised 16 May 2010; accepted 31 May 2010; published 3 Jun 2010

3. Mouse experiments

All animal procedures were in accordance with a Fourth Military Medical University (FMMU) approved animal protocol. Two typical experiments were described as below either mouse model implanted with a luminescent source into the belly or liver tumor xenograft model.

3.1 Experiment based on implanted luminescence source mouse model

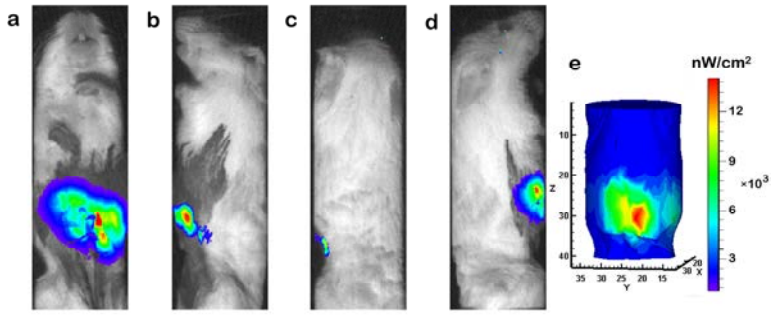

Fig. 2. Multi-view overlay images of photographs and luminescent images and the absolute irradiance distribution on the mouse surface. (a) Anterior-posterior view, (b) right lateral view, (c) posterior- anterior view, (d) left lateral view, and (e) the absolute irradiance distribution on the mouse surface after mapping from 2D luminescent data.

In this experiment, a living mouse was selected as the research object to evaluate the performance of the developed BLT/MicroCT dual modality imaging system and the corresponding reconstruction algorithm. To simulate the bioluminescence source, a luminescent catheter that was made from a luminescent light stick (Glowproducts, Canada) was employed and sewed into the abdomen of the mouse. Because the emission peak wavelength of the luminescent light stick is about 644 *nm*, the optical parameters were calculated at this wavelength based on the literature reports [25] and were listed in Table 1. Multi-view overlay images of photographs and luminescent images were acquired by CCD camera from four directions with 90 degrees intervals, as shown in Fig. 2(a)-(d). In order to combine BLT and MicroCT system, optical data and volume data of MicroCT need to register to the same coordinate as follow. Four small balls of 0.5 *mm* in diameter were used as the marks, which are made of polyethylene. The position information of marks can be read from the volume data which is reconstructed from the original X-ray slices. Meanwhile, two dimensional (2D) coordinates of the same marks on the planar optical photographs can be obtained. In addition, the third coordinate can be calculated through the optical imaging principle with the basic parameters, including the perpendicular distance between the image and the lens system, the distance between the object and the lens system, the focus of the lens system, and the magnification of the optical system. After registering the dual modality data, the absolute irradiance distribution on the mouse surface was mapped based on the inverse process of hybrid radiosity-radinace theorem free-space photon transport model [24]. Besides, the influence of camera lens was further taken into account to eliminate the overlapping problem and the inconsistent data distributions at the same position from different views and shown in Fig. 2(e). During the BLT acquisition in tandem to CT, the mouse retained the same body posture. In order to go through heterogeneous

#126793 - $15.00 USD Received 9 Apr 2010; revised 16 May 2010; accepted 31 May 2010; published 3 Jun 2010

reconstruction, we segmented the MicroCT slices of the mouse to get the anatomical information, such as adipose, heart, lungs, liver, and kidneys using commercially available software Amira 4.1.1 (Mercury Computer system, Inc. Chelmsford, MA). To reduce the ill-posedness of BLT by reducing the numbers of unknown variables, we set a potential permissible source region as $\Omega_s = \{(x, y, z) \mid 0 < x < 100,\ 19 < y < 24,\ 26 < z < 34\}$ according to the flux distribution on the surface in Fig. 2(e). The region of interest in the heterogeneous mouse torso consists of 18837 tetrahedral elements and 3480 nodes, 23497 tetrahedral elements and 4779 nodes in the homogeneous mouse torso.

Table 1. Optical Parameters of the Mouse Organ Regions

Material		Adipose	Heart	Lung	Liver	Kidney	Spleen
620 *nm*	$\mu_a[mm^{-1}]$	0.0086	0.1382	0.4596	0.8291	0.1550	0.8293
	$\mu_s'[mm^{-1}]$	1.2584	1.0769	2.2651	0.7356	2.5329	0.7356
640 *nm*	$\mu_a[mm^{-1}]$	0.0057	0.0910	0.3045	0.5458	0.1021	0.5461
	$\mu_s'[mm^{-1}]$	1.2374	1.0291	2.2273	0.7115	2.4144	0.7115

3.2 Experiments based on tumor-bearing nude mouse models

The firefly luciferase generates visible light in tissues usually through the oxidation of an enzyme specific substrate in the presence of oxygen, such as a cofactor of ATP as a source of energy [31]. Although implanted luminescent stick source can be accurately located by MicroCT, it is, however, very difficult for the source reconstruction of early tumors with report gene probe of firefly luciferase, because the optical signal intensity of report protein is much weaker than that from the Growproducts luminescent source.

In this experiment, male athymic nude mice were obtained from the animal center of FMMU, which were housed in cabinets under germ free condition and used at age of 6 weeks. We chose viable PC3-Luc prostate cancer cell line since the luciferin-luciferase transporter conjugates demonstrated stability and quick release in PC3-Luc cell line in *ex vivo* and *in vivo* experiments [32], which was maintained as a monolayer culture in F12 medium supplement with 10% fetal bovin serum (FBS) and Penicillin-Streptomycin.

Single cell suspensions with a cell viability of >95%, as determined by trypan blue exclusion, were used for injection. The mice were maintained under gaseous anesthesia (isoflurane 1.5%, oxygen $0.3l\ min^{-1}$) in a warmed-up technical cell dedicated to multimodality imaging for small animals. A midline incision was made through abdominal muscles to expose the hepatic lobes. 4×10^5 PC3-Luc cells were mixed with $10\mu l$ Matrigel (BD Matrigel Basement Membrane Matrix, BD Biosciences, NJ) and $10\mu l$ PBS were injected into the right hepatic lobes. The formation of a bleb was the sign of a satisfactory injection, and then the abdomen was closed with single-stitch sutures.

In order to acquire anatomical structure information for heterogeneous reconstruction, mice were injected with $0.25ml / 20g$ of Fenestra blood pool contrast agent (Fenestra LC, ART Advanced Research Technologies Inc., QC, Canada,) into the distal tail vein using a 27-gauge needle. This contrast agent allows contrast enhancement within 4 hours post-injection. D-luciferin in aqueous solution (125 *mg/kg* body weight) was injected into the mouse peritoneal cavity (i.p.) 10 *min* prior to BLT imaging, and then the mouse was placed onto the warmed stage inside the light tight chamber and received continuous exposure under gaseous anesthesia (isoflurane 1.5%, oxygen $0.3l\ min^{-1}$) to sustain sedation during imaging. The same mouse was scanned similarly to get the four overlay images at the time point of day 2 (exposure time 3 *min*, binning 4×4), as shown in Fig. 3. BLT was quantified in unit of total

#126793 - $15.00 USD Received 9 Apr 2010; revised 16 May 2010; accepted 31 May 2010; published 3 Jun 2010

power (*nW*) inside the living mouse. We validated the location of the overlay image at the anterior-posterior posture with the Caliper IVIS Kinetic imaging system (Fig. 5(a)). Four absolute irradiance distributions on the mouse surface were mapped from 2D luminescent data, the anterior-posterior of the four results is shown in Fig. 5 (d). Then, the same reconstruction algorithm based on *hp*-FEM was adopted in our studies of tumor-bearing mouse models. we set a potential permissible source region as $\Omega_s = \{(x, y, z) \mid 0 < x < 23,\ 30 < y < 35,\ 15 < z < 20\}$ as described in the first experiment, the region of interest of the heterogeneous mouse torso (19058 tetrahedral elements and 3677 nodes) is, almost the same as the homogeneous mouse torso (17899 tetrahedral elements and 3842 nodes). Similarly, we segmented the MicroCT slices of the mouse to obtain the anatomical information, such as the heart, lungs, liver, kidneys etc. as described previously. In this reconstruction of tumor-bearing mouse model, all optical parameters at 620 *nm* wavelength [31] were adopted for different organs and tissues. In the homogeneous mouse model analysis, the optical parameters of adipose tissue at 620 *nm* wavelength were adopted in the source reconstruction.

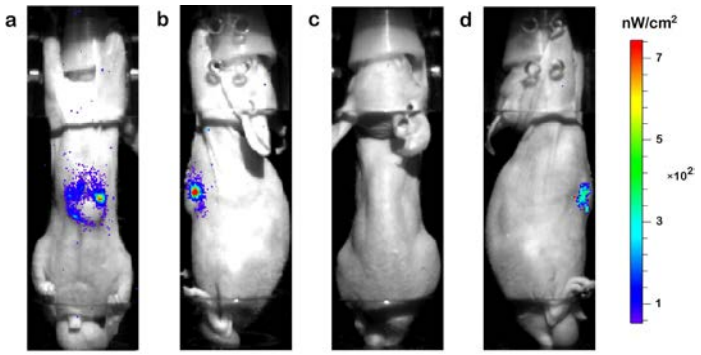

Fig. 3. Four overlay images from bioluminescent images and corresponding photographs of the PC3-Luc cells inoculated to the hepatic lobes of nude mouse. (a) Anterior-posterior, (b) left lateral, (c) posterior-anterior, and (d) right lateral image.

We developed the cell level quantification method based on our calibrated hardware system and reformative *hp*-FEM reconstruction algorithm. Nude mice were injected with different numbers of PC3-Luc cells (1×10^5, 2×10^5, 4×10^5, 6×10^5, 8×10^5, 1×10^6) into the right hepatic lobes. The multi-view images were acquired at the time point of about 20 hours after inoculation of the tumor cells. The total power (*nW*) of tumor cells expressing luciferase gene reporter was thus calculated.

4. Results

The first typical reconstruction results of implanted luminescent source were analyzed between the heterogeneous and homogeneous mouse models. We obtain the actual luminescent source position coordinate is (29.3 *mm*, 22.3 *mm*, 26.6 *mm*). It is clear from Table 2 that the reconstruction results based on heterogeneous mouse model is better than the homogeneous mouse model in localization and quantification. The reconstruction results based on heterogeneous mouse model had very little localization deviation (ca. 0.3 *mm*), and quantitative deviation less than 6.5% at the wavelength of 640 *nm*, which is better than the reported results of 0.85 *mm* and 20% [26]. In contrast, the corresponding reconstruction results based on homogeneous mouse model were 2.37 *mm* in localization deviation and 59.0% in quantitative deviation at the same wavelength, the same permissible source region and the same regularization parameter.

#126793 - $15.00 USD Received 9 Apr 2010; revised 16 May 2010; accepted 31 May 2010; published 3 Jun 2010

Table 2. Comparison of Reconstruction Results Based on Heterogeneous and Homogeneous Mouse Models

	Total power (nW)					Localization deviation (mm)	
Wavelength	p_{real}	p_{heter}	ξ_{heter}	p_{homo}	ξ_{homo}	d_{heter}	d_{homo}
640 *nm*	415	442	6.5%	660	59.0%	0.30	2.37

Note: p_{real} represents the actual total power of the luminescent source, p_{heter} is the total power of heterogeneous mouse reconstruction, p_{homo} is the total power of homogeneous mouse reconstruction, ξ_{heter} is the quantitative deviation of heterogeneous mouse, ξ_{homo} is the quantitative deviation of homogeneous mouse.

The typical reconstruction results of implanted luminescent source are compared with actual source for the heterogeneous and homogeneous mouse models. Figure 4(a) and (b) showed the reconstruction results of implanted source in these two mouse models at the same angle of view, respectively. The heterogeneous coordinate of the reconstructed source with the maximum density is (29.5 *mm*, 22.1 *mm*, 26.7 *mm*), and that of the homogeneous coordinate is (30.7 *mm*, 22.9 *mm*, 28.4 *mm*), thus, we achieved the deviation between the two reconstructed source centers to the actual source center as 0.30 *mm* and 2.37 *mm*, we can find the difference from Fig. 4, Fig. 4(c) and (d) are the amplified images of the reconstruction source and actual source of the Fig. 4(a) and (b), respectively. The blue stick is the actual implanted source including the external figure of plastic catheter, and the tetrahedra near the actual source are reconstructed source. Along with the two reconstruction results, the deviations achieve to 0.1 *mm* and 1.8 *mm* from the Z-axis direction, respectively. The reconstruction of the heterogeneous and the homogeneous mouse models were performed with almost the same setting of several reconstructed parameters. *hp*-FEM on refine grid was adopted and the BLT reconstruction program coded in MATLAB takes about 200 seconds both for the heterogeneous and homogeneous mouse models on our desktop computer (Intel(R) Core(TM) 2 CPU 6300 @ 1.86GHz and 2GB RAM). There is almost no difference in time cost between these two mouse models.

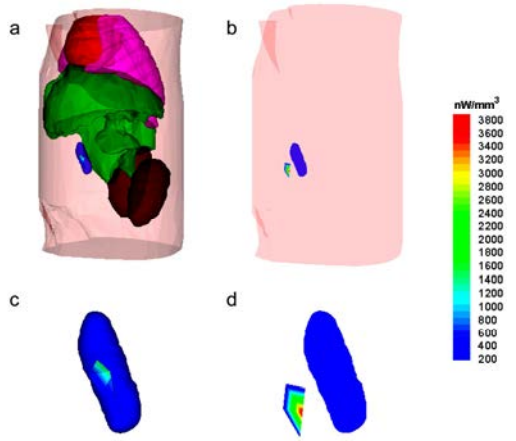

Fig. 4. Typical reconstruction results of implanted luminescent source using the heterogeneous and homogeneous mouse models at the wavelength of 640 *nm*. (a) and (b) are the reconstruction results in the implanted source heterogeneous and homogeneous mouse models, respectively. (c) and (d) are the amplified images of the reconstructed source and actual source of the (a) and (b), respectively. The blue stick is the actual implanted source, and the tetrahedra near the actual source are the reconstructed source.

#126793 - $15.00 USD Received 9 Apr 2010; revised 16 May 2010; accepted 31 May 2010; published 3 Jun 2010

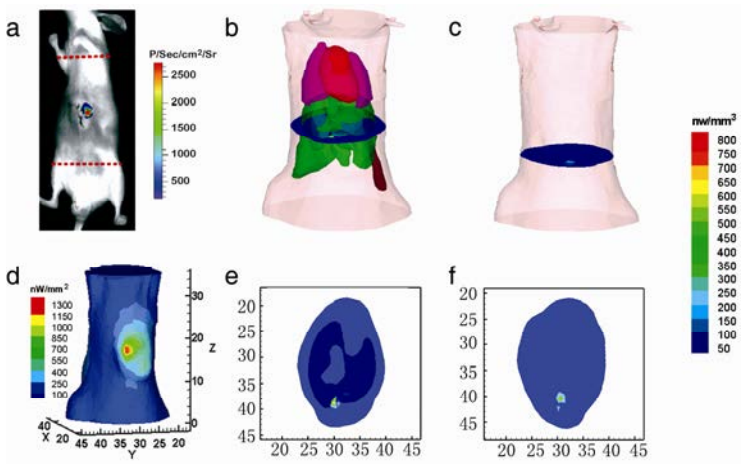

Fig. 5. Comparison of BLI results obtained from Caliper IVIS Kinetic Imaging System and in-house BLT reconstruction results of both heterogeneous and homogeneous BALB/c nude mice tumor-bearing models *in vivo*. (a) Anterior-posterior BLI acquired by IVIS Kinetic imaging system. (b) The reconstruction result based on heterogeneous tumor model. (c) The reconstruction result is based on homogeneous tumor model. (d) The absolute irradiance distribution on the surface of tumor mouse after mapping from 2D luminescent data (Anterior-posterior). (e) and (f) are the slices in the Z-axis direction of reconstructed tumor center of the (b) and (c), respectively.

The second typical reconstruction results of tumor-bearing mouse model experiment were analyzed between the heterogeneous and homogeneous mouse models. The heterogeneous reconstruction result were shown in Fig. 5(b) and the slice in the Z-axis direction of reconstructed tumor's center of the reconstructed source was shown in Fig. 5(e), on the contrary, the homogeneous reconstruction result and its slice were shown in Fig. 5(c) and (f), respectively. We can see the position of tumor in the 3D reconstruction map and slice result. The heterogeneous coordinate of the reconstructed source with the maximum density is (22.5 *mm*, 32.3 *mm*, 16.6 *mm*), and the homogeneous result is (23.5 *mm*, 30.9 *mm*, 19.3 *mm*), thus, we achieved the distance between the two reconstructed source as 3.20 *mm* by the formula of $d = \sqrt{(x-x_0)^2 + (y-y_0)^2 + (z-z_0)^2}$ between heterogeneous and homogeneous mouse models, from the coordinates of the reconstructed maximum source density, the great localization deviation (2.6 *mm*) came from in Z-axis direction. In quantification aspect, the total power of heterogeneous and homogeneous mouse model is 7.8 *nW* and 15.3 *nW*, respectively. The reconstructions took about 100 seconds both the same for the heterogeneous and homogeneous mouse models with the same desktop computer as the first experiment.

Reconstructed total power can reflect the total cell number, but no report of BLT quantification of cell number *in vivo*. We inoculated different number of PC3-Luc cells into the hepatic lobes of mice and constructed the images using a heterogeneous model. Figure 6(a) showed the results of the cell number and the corresponding reconstructed total power. Quantification of tumor cell signal indicated a robust correlation between reconstructed total power and the tumor cell number (R^2 = 0.99) through fitting with a linear function (y = 44402x + 19491) (Fig. 6(b)). On the contrary, BLI results cannot obtain an ideal linear fitting result (y = 0.6516x + 432761, R^2 = 0.09, (Fig. 6(b)). This may be caused by the different depth of tumor in the tumor-bearing mouse models, whereas we try to inoculate tumor cells at the same depth.

#126793 - $15.00 USD Received 9 Apr 2010; revised 16 May 2010; accepted 31 May 2010; published 3 Jun 2010

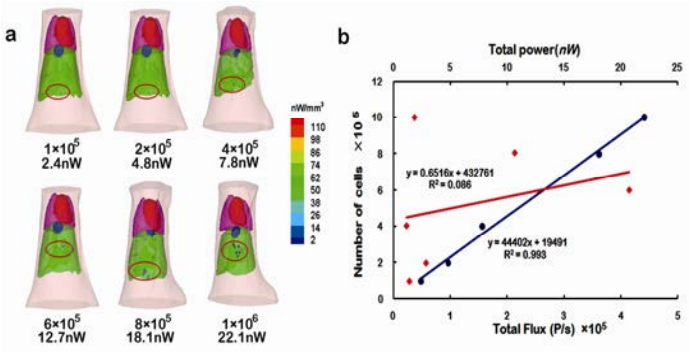

Fig. 6. *In vivo* reconstructions of total power for different cell numbers were performed with our BLT system based on heterogeneous tumor-bearing BALB/c nude mouse models, and the relationship was extracted between total power and tumor cell number. (a) Total power reconstruction of mice with different number of injected cells, the regions within red ellipse are the reconstructed tumors. (b) The relationship between the total power and tumor cell number in BLT (blue line) and total flux in the same size region of interest with different tumor cells number in BLI (red line).

5. Discussions and conclusion

We successfully conducted *in vivo* quantitative and localization research based on heterogeneous and homogeneous mouse models with our newly developed prototype dual modality BLT/MicroCT imaging system and quantitative reconstruction methodology.

The first BLT system for data acquisition was reported by Wang et al. [33], combined multimodality platform further improved the reconstruction and visualization of data [10]. A reformative dual modality BLT system with MicroCT co-registration was developed in our laboratory. It improves reconstruction accuracy and benefits 3D volumetric data registering without mouse atlas to keep the same body posture, especially this fusion technique facilitates the operation and keeps small animal alive during the whole experimental process. The combination of BLT and MicroCT provides a new detection tool with high sensitivity and specificity that facilitates longitudinal monitoring.

We developed the quantitative reconstruction algorithm based on multilevel adaptive finite element algorithm [15] and adaptive *hp*-FEM reconstruction algorithm [16]. The calibration formula for the CCD camera was proposed in this study utilizing integrated sphere standard source system, the effect of the field of view and distance from the source to the CCD camera were considered. Source density unit was adopted to evaluate the reconstruction results by Lv et al. [11], in this study we performed reconstruction results with total power (*nW*), which is more robust than source density. We also showed that tumor depth in the liver lobes can be detected at low cell numbers in mouse models, which is critical for early detection, residual tumor monitoring and early metastasis delineation. Furthermore, this is the first study to establish the linear relationship between the number of tumor cells and the reconstructed total power from BLT. In addition, total power quantification is not limited by the tumors positioned in different depths in mice. For example, in the second experiment, the reconstructed total power is 7.8 *nW*, so we can calculate the tumor cell number *in vivo* through the cell number quantitative function y = 44402x + 19491, and found that the cell number is 3.66×10^5, which coincides with literature report of host versus graft reaction during the first week of tumor inoculation [34,35]. Such robust and accurate quantification would permit us to analyze tumor cell proliferation and apoptosis *in vivo* longitudinally. While BLI cannot provide a good linear relationship between total flux and cell number, because it has no capacity to reveal the depth information inside the small living animal.

The first experimental data showed the more accurate reconstruction results are achieved based on the heterogeneous mouse model than homogeneous one. At the same time, accurate optical parameters are another important factor for the ideal reconstruction. It can reach the

#126793 - $15.00 USD Received 9 Apr 2010; revised 16 May 2010; accepted 31 May 2010; published 3 Jun 2010

0.3 *mm* deviation for localization and 6.5% quantitative deviation at 640 *nm* wavelength based on the heterogeneous mouse model.

There are some new understandings from the comparison of reconstruction deviations came from the heterogeneous model and the homogeneous models in the first experiment. The deviation of 2.37 *mm* in homogeneous is much larger than 0.30 *mm* in heterogeneous model. Especially, we found that the main localization deviation is about 1.8 *mm* in the Z-axis direction in the homogeneous mouse model, while it is only 0.1 *mm* deviation in the heterogeneous mouse model. The similar deviation trends can be observed in the second experiment. Both of the experimental results show that the great difference of the heterogeneous organs in spatial distribution may be the intrinsic reason which causes the great deviation in Z-axis direction. Consequently, the reconstruction deviation in the heterogeneous mouse models may be simultaneously determined by the spatial distribution of heterogeneous organs relative to the actual position of source and corresponding optical properties of organs.

The experiments also show that the method is computationally efficient and of almost equivalent time cost between the heterogeneous and homogeneous mouse models. The quantitative *hp*-finite element reconstruction method can handle a complex heterogeneous geometrical model, suitable for small animals that have complicated anatomies.

There are several limitations of this study. First we have to admit that the post-processing of semi-automatic segmentation is rather time-consuming. Another limitation of the second experiment is that super-early tumors cannot be accurately positioned with the assistance of MicroCT, due to the poor density contrast between the tumor tissue and normal hepatic tissue. The issue of semi-automatic segmentation may be solved by developing effective ways and the localization of actual position of super-early tumors may be solved if we consider using appropriate contrast agent enhancing method. Certainly, further studies of actual source location of super-early tumor are still needed.

In conclusion, we have developed a highly sensitive dual modality BLT/MicroCT system, with which the mouse experiments demonstrated that heterogeneous reconstructions have higher accuracy both in localization and quantification than the homogeneous mouse models with appropriate optical parameters. Moreover, the tumor tomographic reconstruction based on heterogeneous mouse model suggested that BLT technology is feasible for the localization and quantification of very small number of tumor cells. Overall, BLT/MicroCT imaging method offers the advantages of cost-effectiveness, good molecular specificity and sensitivity for noninvasive 3D imaging, and consequently enormous potential in drug development and preclinical oncological investigations.

Acknowledgements

This work is supported by the Program of the National Basic Research and Development Program of China (973) under grant 2006CB705700, the Chang Jiang Scholars and Innovative Research Team in University (PCSIRT) under grant IRT0645, the Chair Professors of Chang Jiang Scholars Program of Ministry of Education of China, CAS Hundred Talents Program, the National Natural Science Foundation of China under grants 30873462, 30900334, 30970845, the Shaanxi Provincial Natural Science Foundation Research Project under grant 2009JQ8018, and the Fundamental Research Funds for the Central Universities.

#126793 - $15.00 USD Received 9 Apr 2010; revised 16 May 2010; accepted 31 May 2010; published 3 Jun 2010